

Med-Tuning: A New Parameter-Efficient Tuning Framework for Medical Volumetric Segmentation

Jiachen Shen^{*1}

M202110559@XS.USTB.EDU.CN

Wenxuan Wang^{*1}

S20200579@XS.USTB.EDU.CN

¹ School of Automation and Electrical Engineering, University of Science and Technology Beijing

Chen Chen²

CHEN.CHEN@CRCV.UCF.EDU

² Center for Research in Computer Vision, University of Central Florida

Jianbo Jiao³

J.JIAO@BHAM.AC.UK

³ School of Computer Science, University of Birmingham

Jing Liu⁴

JLIU@NLPR.IA.AC.CN

⁴ Institute of Automation, Chinese Academy of Sciences

Yan Zhang¹

Shanshan Song¹

Jiangyun Li^{†1}

LEEJY@USTB.EDU.CN

Editors: Accepted for publication at MIDL 2024

Abstract

The “pre-training then fine-tuning (FT)” paradigm is widely adopted to boost the model performance of deep learning-based methods for medical volumetric segmentation. However, conventional full FT incurs high computational and memory costs. Thus, it is of increasing importance to fine-tune pre-trained models for medical volumetric segmentation tasks in a both effective and parameter-efficient manner. In this paper, we introduce a new framework named Med-Tuning to realize parameter-efficient tuning (PET) for medical volumetric segmentation task and an efficient plug-and-play module named Med-Adapter for task-specific feature extraction. With a small number of tuned parameters, our framework enhances the 2D baselines’s precision on segmentation tasks, which are pre-trained on natural images. Extensive experiments on three benchmark datasets (CT and MRI modalities) show that our method achieves better results than previous PET methods on volumetric segmentation tasks. Compared to full FT, Med-Tuning reduces the fine-tuned model parameters by up to 4×, with even better segmentation performance. Our project webpage is at <https://rubics-xuan.github.io/Med-Tuning/>.

Keywords: Parameter-Efficient Tuning, Medical Volumetric Segmentation, Transformer.

1. Introduction

Medical volumetric segmentation (MVS) task is to identify tumors and organ sub-regions in biomedical images, aiding accurate clinical diagnoses and treatment planning. It is crucial in medical research, due to the widespread use of 3D imaging like computed tomography (CT) and magnetic resonance imaging (MRI). In the last decades, a large number of deep neural network architectures have been proposed, including convolutional neural networks (CNNs) (e.g., (Milletari et al., 2016; Çiçek et al., 2016; Isensee et al., 2021)) and Transformer-based networks (e.g., (Cao et al., 2022; Hatamizadeh et al., 2022b,a;

* Contributed equally

† Corresponding author

Zhou et al., 2023; Peiris et al., 2022)). Recently, the “pre-training then fine-tuning” paradigm (Yosinski et al., 2014) has gained much popularity to enhance model performance in downstream tasks. As in (Cao et al., 2022), the conventional full fine-tuning scheme updates all parameters of the pre-trained models. Yet, as models continuously improve in performance, particularly Transformer-based ones like (Cao et al., 2022; Hatamizadeh et al., 2022b,a), their tuned parameter count escalates significantly. Thus, full fine-tuning involves a lot of tuned parameters and entails great training costs. To reduce tuned parameters, head-tuning (Head) was proposed (He et al., 2022), focusing solely on optimizing the task-specific decoder, albeit resulting in decreased model performance. Meanwhile, recent studies (Jia et al., 2022; Chen et al., 2022; Pan et al., 2022; Sung et al., 2022; Yu et al., 2022; Zhang et al., 2023; Xu et al., 2023; Wu et al., 2023; Fischer et al., 2024) focus on parameter-efficient tuning (PET) to balance model performance and tuned parameters.

In this paper, we aim to investigate how to adapt strong visual foundation models pre-trained on natural images to MVS tasks via PET. We initiate our analysis with some examples of widely available models that use image-level pre-training (e.g., classification task (Deng et al., 2009), CLIP (Radford et al., 2021), MOCO v3 (Chen et al., 2021)) in natural image domain. Figure 1 presents the two-

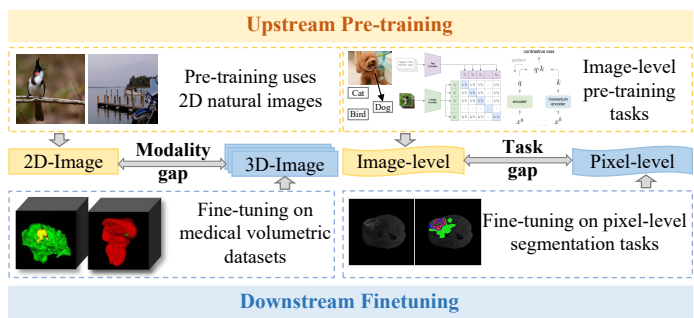


Figure 1: The two-fold gaps between upstream pre-training and our downstream fine-tuning.

fold gaps between upstream pre-training and downstream fine-tuning: (1) **Domain gap** between natural images and medical volumes; (2) **Task gap** between image-level pre-training and pixel-level segmentation. To narrow these gaps, we propose **Med-Tuning**, a new PET framework for MVS, and **Med-Adapter**, an efficient plug-and-play module for task-specific feature extractions. Med-Tuning processes 3D volumes through a frozen pre-trained Transformer model with inserted Med-Adapters. Med-Adapter greatly narrow both gaps by capturing spatial multi-scale features and volumetric correlations between slices with few additional parameters. Our main contributions are summarized as follows:

- We propose a new PET framework **Med-Tuning**, which greatly boosts the performance of the pre-trained models on MVS task and reduces training costs.
- We propose a plug-and-play module **Med-Adapter**, to consider both spatial relationship modeling (coarse/fine-grained) and volumetric correlations between slices.
- Extensive experiments on three benchmark datasets with both CT and MRI modalities convince the effectiveness of **Med-Tuning** over full fine-tuning and other PET methods.
- **Med-Tuning** adapts well to the rapidly evolving Transformer-based visual foundation models (i.e., SAM), showcasing strong generalization and flexibility.

2. Related Work

2.1. Medical Volumetric Segmentation

Achieving promising performance on MVS requires the incorporation of both spatial multi-scale representations and volumetric correlations, as demonstrated by prior research (Hatamizadeh

et al., 2022a). Several U-Net inspired CNN-based models (Ronneberger et al., 2015; Çiçek et al., 2016; Zhou et al., 2018; Isensee et al., 2021) concatenate multi-scale features from the encoder and up-sampled features, complementing the loss of spatial information caused by down-samplings. Cao et al. (Cao et al., 2022) use skip connections to effectively fuse low-level and high-level features in Transformers. Besides, various MVS methods capture volumetric correlations by 3D convolutions (Çiçek et al., 2016; Milletari et al., 2016; Isensee et al., 2021) or self-attention mechanism among 3D volumes (Wang et al., 2021).

2.2. Visual Parameter-Efficient Tuning

Recently, novel vision PET methods have emerged to balance accuracy and tuned parameter efficiency during fine-tuning, which can be categorized into three groups: **(1)** Prompt-based methods (Zhang et al., 2023; Fischer et al., 2024). For instance, VPT (Jia et al., 2022) adds learnable prompt tokens to patch embeddings for downstream visual tasks. Pro-tuning (Nie et al., 2023) inserts multiple stage-wise prompt blocks into different stages of the backbone. **(2)** Adapter-based methods (Houlsby et al., 2019; Chen et al., 2022; Yang et al., 2023; Wu et al., 2023). Adapter is a lightweight module inserted between the feed-forward layer and layer normalization in Transformer, which are tuned during fine-tuning while other layers stay frozen. ST-Adapter (Pan et al., 2022) introduces 3D depth-wise convolution (DWConv) (Ye et al., 2019) in Adapter modules to capture spatial-temporal features. **(3)** Other PET techniques. SAN (Xu et al., 2023) is a small and separate network that is trained via shortcut connections from backbone to reduce memory cost during fine-tuning. Recent studies (Wu et al., 2023; Chai et al., 2023) mainly focus on exploring the potential of the Segment Anything Model (SAM) for medical image analysis.

2.3. Utilization of Fourier Transform in Computer Vision

Image analysis in Fourier domain is extensively used in various vision tasks (Ding et al., 2017; Lee et al., 2018; Li et al., 2020; Chi et al., 2020; Yang and Soatto, 2020; Rao et al., 2021). Fast Fourier Transform (FFT) and Inverse Fast Fourier Transform (IFFT) leverage frequency information for global connectivity through parameter-free domain mapping on original images, resulting in an intrinsic global vision characteristic. According to the conclusion of (Oppenheim et al., 1979; Liu et al., 2023a), the phase-only image or feature retains many of the semantics features of the original image.

3. Methodology

3.1. Preliminaries

Vanilla Adapter. Given an input feature $X \in \mathbb{R}^{N \times d}$, the vanilla Adapter can be represented as Equation (1) (Houlsby et al., 2019), where W_{down} and W_{up} indicate the down-projection and up-projection layer, $\sigma(\cdot)$ is an activation function, $+$ is a skip-connection.

$$\text{Adapter}(X) = X + \sigma(XW_{down})W_{up}, \quad (1)$$

Discrete Fourier Transform. Discrete Fourier Transform (DFT) serves as classical technique for computer vision applications (Rao et al., 2021). Given a 3D input (volumetric data or feature) $x[D, H, W]$, DFT is defined as:

$$X = \mathcal{F}(x) = \sum_{w=0}^{W-1} \sum_{h=0}^{H-1} \sum_{d=0}^{D-1} x(d, h, w) e^{-j2\pi(\frac{xd}{D} + \frac{yh}{H} + \frac{zw}{W})} = \mathcal{R} + \mathcal{I}j, \quad (2)$$

where X is a complex matrix, \mathcal{R} and \mathcal{I} denote its real and imaginary part. In implementation, we use the accelerated versions of DFT and Inverse DFT (i.e., FFT and IFFT).

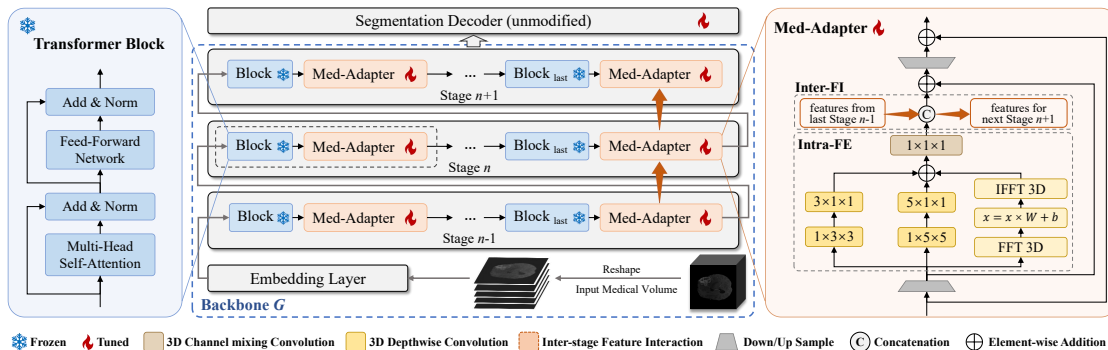


Figure 2: The overall architecture of Med-Tuning. Med-Tuning consists of a 2D Transformer baseline with proposed Med-Adapters inserted at each encoder stage. Only Med-Adapters and decoder are **tuned** while all the other layers stay **frozen**.

3.2. Med-Tuning: Parameter-Efficient Tuning for MVS

The overall architecture of our framework is depicted in Figure 2. Med-Tuning consists of a 2D Transformer backbone G pre-trained on natural images, a segmentation decoder and inserted Med-Adapter. Given a batch of medical volumes input $I[B, C, D, H, W]$, (B, C, D, H, W is the number of batch size, channel, slice, height, width), we initially reshape them to $I[BD, C, H, W]$ before embedding layer. According to two main considerations in the following, we decide to exclusively introduce Med-Adapter into encoder without modifying decoder, enabling high decoder scalability to meet different requirements. First, encoder plays a pivotal role in baseline. Inadequate feature extraction will hinder performance even with the same robust decoder, as evidenced by the decline in results for Head compared to Full, detailed in Table 1, Table 2 and Table 3. Besides, not all segmentation decoders come with pre-trained weights, necessitating the fine-tuning of the entire decoder. Secondly, sole insertion in encoder part improves the flexibility of the whole framework. Our inserting strategy broadens the adaptability of Med-Tuning on visual foundation models while reducing tuned parameters.

3.3. Med-Adapter: Adapter for MVS

We propose a task-oriented and simple yet effective module for medical volumetric data, namely **Med-Adapter**. The motivation of Med-Adapter is to empower a 2D Transformer model pre-trained on natural images to gain the capability of volumetric feature modeling in a parameter-efficient manner. Here we consider three criteria when designing Med-Adapter: (1) *MVS oriented*: It’s necessary to narrow the mentioned gaps in Figure 1. (2) *Light-weight*: Structure with a low amount of parameters is crucial. (3) *Plug-and-play*: An easy-to-implement module is friendly to practical deployment. While retaining the bottleneck structure of the vanilla Adapter (Equation (1)), we introduce a few tailored designs into Med-Adapter based on above criteria, shown in Figure 2 (right).

3.3.1. INTRA-STAGE FEATURE ENHANCEMENT (INTRA-FE).

We introduce multiple branches tailored to capture fine-grained feature representations, coarse-grained global semantics and volumetric correlations among slices, which are vital for realizing accurate medical volumetric segmentation task.

Multi-scale Local Branch (MLB) We employ parallel 3D convolutions with kernels of sizes $k = 3$ and $k = 5$ to extract spatial multi-scale features and 3D volumetric correlations between slices. The conventional 3D convolution operations are replaced with 3D DWConv in a parameter-efficient manner. Moreover, we use two cascaded $1 \times k \times k$ and $k \times 1 \times 1$ convolutions to replace the $k \times k \times k$ convolution to pursue an extremely lightweight structure.

FFT Global Branch (FGB) To achieve coarse-grained global semantic extraction in a parameter-efficient way, we substitute traditional large convolutional kernels and attention mechanisms, known for their memory and computation demands, with 3D FFT, IFFT and learnable complex matrices. These filter-like complex matrices are designed to model frequency features that contain global semantics in the whole frequency domain. Compared to vanilla 3D self-attention operation with $\mathcal{O}(n^3)$ complexity (n is the number of tokens), our FGB is a lightweight module. In detail, the computational complexity of FGB is $\mathcal{O}(n \log(n))$, where FFT and IFFT are both with $\mathcal{O}(n \log(n))$ complexity while that of Hadamard product or matrix addition is $\mathcal{O}(n)$. Then we merge the aforementioned branches by efficient $1 \times 1 \times 1$ convolution. Therefore, given the intermediate embedded feature representations $X \in [BD, C', HW]$, the Intra-FE module can be expressed as Equation (3)-(5). In this way, the Intra-FE module is theoretically capable of modeling volumetric correlations among slices and incorporating abundant spatial multi-scale features for the downstream dense prediction task (i.e., MVS).

$$\text{Intra-FE} = M = \text{Conv}_{1 \times 1 \times 1}(\text{MLB} + \text{FGB}), \quad (3)$$

$$\text{MLB} = \text{DWConv}_3(X') + \text{DWConv}_5(X'), \text{ FGB} = \mathcal{F}^{-1}(W_F \odot \mathcal{F}(X') + b_F) \quad (4)$$

$$X' = \text{R}_{\text{volume}}(\sigma(XW_{\text{down}})), X' \in [B, C', D, H, W], C' = C/\alpha \quad (5)$$

where M is the intra-stage enhanced feature representations. W_F and b_F are the learnable complex matrices, \mathcal{F} is 3D FFT in Equation (2) and \mathcal{F}^{-1} is 3D IFFT. \odot is the hadamard product, while R_{volume} is a reshape operation to obtain cube-shape feature representations.

3.3.2. INTER-STAGE FEATURE INTERACTION (INTER-FI).

To fully exploit the representations collected by Inter-FI modules in Med-Adapter at each stage, we further consider the feature interaction between different stages. The intra-stage enhanced feature representations M in this stage will be fused with $M_{\text{LastStage}}$ (i.e., the output of the Intra-FE module from the previous stage). Note that Inter-FI is only introduced at specific Med-Adapters at the end of each stage. Thus, Inter-FI is expressed as Equation (6). In this way, feature representations extracted by Intra-FE modules of Med-Adapters in shallow layers are gradually fed to adjacent higher layers, realizing inter-stage feature interaction by explicit enhancement and thus boosting model performance.

$$\text{Inter-FI} = \text{Cat}(\mathcal{A}(H, M_{\text{LastStage}})), M = \begin{cases} \text{Inter-FI}, & \text{if } \text{Flag}_{\text{last}} \\ M, & \text{if not } \text{Flag}_{\text{last}} \end{cases} \quad (6)$$

where \mathcal{A} denotes convolution operations to align M and $M_{\text{LastStage}}$ in terms of spatial resolution and channel dimension, Cat refers the concatenation. $\text{Flag}_{\text{last}}$ is a bool parameter and $\text{Flag}_{\text{last}} = \text{True}$ when the current Med-Adapter is the inserted last one at this stage.

In summary, our Med-Adapter can be formulated as Equation (7). $\text{R}_{\text{flatten}}$ denotes a symmetric operation that reshapes the feature back to the original shape of X .

$$\text{Med-Adapter}(X) = X + \text{R}_{\text{flatten}}(M + \text{R}_{\text{volume}}(\sigma(XW_{\text{down}}))W_{\text{up}}). \quad (7)$$

4. Experiments and Results

4.1. Experimental Setup

Datasets and Evaluation Metrics. Our proposed Med-Tuning is evaluated on three benchmark datasets: **(1)** Kidney Tumor Segmentation 2019 (Heller et al., 2019)(KiTS 2019), **(2)** Brain Tumor Segmentation 2019 (BraTS 2019) (Menze et al., 2014; Bakas et al., 2017, 2018), **(3)** Brain Tumor Segmentation 2020 (BraTS 2020) (Menze et al., 2014; Bakas et al., 2017, 2018), detailed in [Appendix A.1](#). KiTS 2019 dataset comprises multi-phase 3D CTs depicting the kidneys and tumors. The ground truth contains 3 classes: background (label 0), kidney (label 1), and kidney tumor (label 2). The segmentation accuracy of KiTS 2019 is measured by kidney dice (label 1 and 2) and tumor dice (label 2), composite dice (the average of kidney and tumor dice). BraTS 2019 and BraTS 2020 datasets consist of 3D brain MRI scans with four modalities. The ground truth contains 4 classes: background (label 0), necrotic and non-enhancing tumor (label 1), peritumoral edema (label 2), and GD-enhancing tumor (label 4). The segmentation accuracy is measured by Dice score and the Hausdorff distance (95%) metrics for enhancing tumor region (ET, label 4), regions of tumor core (TC, labels 1 and 4), and whole tumor region (WT, labels 1,2 and 4).

Implementation Details. Experiments utilizing PyTorch (Paszke et al., 2019) for implementation are conducted on NVIDIA GeForce RTX 3090 GPUs. The pre-trained vanilla ViT (Dosovitskiy et al., 2021) with UPerNet (Xiao et al., 2018) decoder (ViT+UPerNet) and Swin-UNet (Cao et al., 2022) based on pre-trained Swin Transformer(tiny) are our chosen baselines. More implementation details are available in [Appendix A.2](#).

4.2. Results and Analysis

We conduct experiments on three benchmark validation sets and compare our method with scratch (i.e., training with random initialization, without pre-training), full fine-tuning, head tuning and previous state-of-the-art PET approaches (i.e., VPT (Jia et al., 2022), Adapter (Houlsby et al., 2019), AdaptFormer (Chen et al., 2022), Pro-tuning (Nie et al., 2023), ST-Adapter (Pan et al., 2022)). Qualitative results are shown in [Appendix B](#).

KiTS 2019. The performance comparisons with ViT+UPerNet and Swin-UNet as baseline are shown in Table 1. Our proposed method boosts the performance of full fine-tuning considerably and achieves much higher Dice scores than previous PET methods, with much fewer tuned model parameters. In comparison with recently proposed PET methods (e.g., VPT, Pro-tuning and ST-Adapter), our Med-Tuning achieves better performance-efficiency trade-off on two baselines. Specifically, Med-Tuning improves model performance by a large margin (i.e., $\uparrow 4.20\%$ Kidney Dice, $\uparrow 17.13\%$ Tumor Dice, $\uparrow 10.67\%$ Composite Dice on ViT+UPerNet and $\uparrow 1.01\%$ Kidney Dice, $\uparrow 8.02\%$ Tumor Dice, $\uparrow 4.52\%$ Composite Dice on Swin-UNet) with only **17.70%** and **27.58%** of tuned parameters respectively in comparison with full fine-tuning.

BraTS 2019. Performance comparisons on BraTS 2019 on two baselines are shown in Table 2 (left) and Table 3 (left). Results show that our method attains the best trade-off between performance and efficiency, achieving comparable or even better results than previous methods. Compared to full fine-tuning, Med-Tuning achieves maximum improvements of **4.23%** (ViT+UPerNet) and **1.28%** (Swin-UNet) in Dice scores. Our Med-Tuning also achieves high parameter efficiency, tuning only **17.70%** parameters of ViT and **27.58%** of Swin-UNet, with inserted parameters being only **2.82%** of ViT and **2.72%** of Swin-UNet.

Table 1: Performance comparison on KiTS 2019 with Swin-UNet and ViT+UPerNet. **Blue** and **Green** text denote the percentage of tuned parameters and the performance improvement compared to full fine-tuning (with grey background).

KiTS 2019	ViT+UPerNet					Swin-UNet				
	Tuned	Inserted	Dice (%) \uparrow			Tuned	Inserted	Dice (%) \uparrow		
	Params(M)	Params(M)	Kidney	Tumor	Composite	Params(M)	Params(M)	Kidney	Tumor	Composite
Scratch	100.849	-	88.01	46.53	67.27	27.154	-	94.33	61.10	77.71
Full	100.849	-	87.32	47.34	67.33	27.154	-	94.68	62.13	78.40
Head	15.007	-	87.35	42.85	65.10	6.752	-	91.95	53.93	72.94
VPT-Shallow	15.015	0.008	86.91	41.67	64.29	6.753	0.001	91.72	54.86	73.29
VPT-Deep	15.100	0.092	88.01	46.45	67.23	6.780	0.029	91.53	53.41	72.47
Adapter	18.567	3.560	89.75	49.03	69.39	7.541	0.790	93.02	57.15	75.08
AdaptFormer	16.197	1.190	87.62	44.46	66.04	7.124	0.372	93.74	59.79	76.77
Pro-tuning	19.812	4.805	89.44	48.32	68.88	8.359	1.607	90.34	51.19	70.77
ST-Adapter	22.118	7.110	90.33	61.29	75.81	8.328	1.577	92.97	57.33	75.15
Ours	17.853 17.70%	2.846 2.82%	91.52 (+4.20)	64.47 (+17.13)	78.00 (+10.67)	7.489 27.58%	0.738 2.72%	95.69 (+1.01)	70.14 (+8.01)	82.92 (+4.52)

Table 2: Performance comparison on BraTS 2019 and BraTS 2020 with ViT+UPerNet.

ViT+UPerNet	Tuned	Inserted	BraTS 2019						BraTS 2020					
	Params	Params	Dice (%) \uparrow			Hausdorff (mm) \downarrow			Dice (%) \uparrow			Hausdorff (mm) \downarrow		
	(M)	(M)	ET	WT	TC	ET	WT	TC	ET	WT	TC	ET	WT	TC
Scratch	100.849	-	64.96	83.03	71.34	7.64	10.60	10.94	65.80	83.72	72.01	32.48	10.06	21.47
Full	100.849	-	68.49	85.56	75.12	6.67	7.88	10.53	69.12	85.90	75.29	34.43	7.32	17.09
Head	15.007	-	65.71	84.19	74.77	6.13	7.51	7.86	66.03	84.50	74.47	37.81	7.47	14.15
VPT-Shallow	15.015	0.008	66.02	84.72	75.84	6.11	7.51	8.47	66.52	84.82	75.46	37.77	7.47	13.53
VPT-Deep	15.100	0.092	67.01	85.14	76.80	6.06	7.72	7.65	67.69	85.28	76.59	31.77	7.74	10.62
Adapter	18.567	3.560	68.30	85.37	77.05	5.50	7.64	7.99	68.58	85.77	77.00	32.63	8.17	16.18
AdaptFormer	16.197	1.190	65.88	84.34	74.77	6.65	8.20	8.43	65.52	84.14	74.28	41.03	8.39	14.78
Pro-tuning	19.812	4.805	67.18	85.32	76.51	5.81	7.07	7.56	67.28	85.57	76.58	40.43	7.00	12.87
ST-Adapter	22.118	7.110	69.18	86.27	79.18	6.08	6.94	6.78	68.60	86.55	79.52	34.06	6.79	12.77
Ours	17.853 17.70%	2.846 2.82%	70.53 (+2.04)	86.58 (+1.02)	79.35 (+4.23)	5.86 (-0.81)	6.22 (-1.66)	6.95 (-3.58)	70.69 (+1.57)	86.69 (+0.79)	79.36 (+4.07)	28.64 (-5.79)	6.20 (-1.12)	15.05 (-2.04)

BraTS 2020. Performance comparisons on BraTS 2020 are shown in Table 2 (right) and Table 3 (right). Compared to full fine-tuning, Med-Tuning achieves maximum improvements of **4.07%** (ViT+UPerNet) and **1.64%** (Swin-UNet) in Dice scores with very few tuned parameters, surpassing most of PET methods. Compared to ST-Adapter, our tuned parameters are fewer yet yield a more substantial overall performance improvement. Moreover, Med-Tuning took about 1.34 (ViT+UPerNet) and 1.68 (Swin-UNet) hours for fine-tuning, 0.76 (ViT+UPerNet) and 0.46 (Swin-UNet) minutes per sample for inference.

Table 3: Performance comparison on BraTS 2019 and BraTS 2020 with Swin-UNet.

Swin-UNet	Tuned	Inserted	BraTS 2019						BraTS 2020					
	Params	Params	Dice (%) \uparrow			Hausdorff (mm) \downarrow			Dice (%) \uparrow			Hausdorff (mm) \downarrow		
	(M)	(M)	ET	WT	TC	ET	WT	TC	ET	WT	TC	ET	WT	TC
Scratch	27.154	-	78.38	88.59	76.46	6.06	10.65	9.18	78.72	89.12	77.07	7.62	6.98	19.08
Full	27.154	-	78.26	89.56	79.16	4.33	6.15	6.70	79.09	89.87	79.15	9.67	6.03	15.31
Head	6.752	-	78.07	88.68	77.26	5.02	6.70	7.09	78.77	88.66	76.90	4.89	8.49	16.06
VPT-Shallow	6.753	0.001	77.16	88.30	76.77	5.42	6.15	7.35	77.43	88.23	76.13	7.53	6.07	16.07
VPT-Deep	6.780	0.029	77.02	88.65	76.91	5.30	7.09	7.94	78.63	88.80	77.17	8.27	6.23	13.25
Adapter	7.541	0.790	77.98	89.22	78.02	5.30	6.62	8.49	78.51	89.16	77.71	7.05	6.25	19.09
AdaptFormer	7.124	0.372	77.69	88.61	76.83	4.91	6.29	7.89	78.22	88.92	76.40	10.35	6.48	16.90
Pro-tuning	8.359	1.607	78.58	89.33	78.79	5.27	6.41	8.24	78.77	89.46	78.20	7.31	6.50	10.54
ST-Adapter	8.328	1.577	78.40	89.54	77.44	4.75	6.01	7.41	78.96	89.54	77.85	7.67	5.48	15.53
Ours	7.489 27.58%	0.738 2.72%	78.51 (+0.25)	89.68 (+0.12)	80.44 (+1.28)	4.00 (-0.33)	5.52 (-0.63)	5.76 (-0.94)	79.25 (+0.16)	90.06 (+0.19)	80.79 (+1.64)	12.40 (+2.73)	4.41 (-1.62)	11.59 (-3.72)

4.3. Ablation Studies

Extensive ablation experiments are conducted based on five-fold cross-validation. For more ablation experiments please refer to [Appendix C](#).

Inserted Position of Med-Adapter.

We conduct experiments on BraTS 2019 training set to assess the segmentation performance by inserting Med-Adapter at various stages of Swin-UNet encoder. Given that Swin-UNet encoder has four continuous stages ($n = 0, 1, 2, 3$). According to [Table 4](#), Inserting Med-Adapter in the initial stages resulted in degraded performance, with none surpassing our best default setting (gray background). This may be attributed to the greater contribution of features learned in later encoder stages when transferring pre-trained weights to the MVS task.

Generalization Capability on Other Pre-trained Weights. To explore the potential of our Med-Tuning, we investigate the effect of diverse encoder pre-trained weights (e.g., multi-modal based (CLIP (Radford et al., 2021)), self-supervised based (MAE (He et al., 2022)), MoCo v3 (Chen et al., 2021)) and SAM (Kirillov et al., 2023)) on BraTS 2019 training set with ViT-B/16. As presented in [Table 5](#), given different pre-trained weights, our easy-to-integrate framework boosts the performance consistently with much fewer tuned parameters, suggesting the effectiveness and robustness of our Med-Tuning framework.

Generalization Capability on 3D Baseline and Medical Pre-trained Weight. To demonstrate the generalization capability of our approach, we select Swin UNETR (Tang et al., 2022) pre-trained on medical datasets as a supplementary 3D baseline and experiment on part of the Medical Segmentation Decathlon (MSD) (Antonelli et al., 2022) dataset. For implementation details please refer to [Appendix A.3](#). Experimental results in [Table 6](#) show that our method still outperforms full fine-tuning in Memory, Time and Dice score.

Table 4: Ablation study on the position of inserted Med-Adapter.

Encoder $n=0$ $n=1$ $n=2$ $n=3$	Dice (%) \uparrow			HF (mm) \downarrow		
	ET	WT	TC	ET	WT	TC
- - - -	78.07	88.68	77.26	5.02	6.70	7.10
\checkmark - - -	-	-	-	-	-	-
\checkmark \checkmark - -	74.83	87.09	72.94	7.26	13.12	10.17
\checkmark \checkmark \checkmark -	75.60	86.79	73.41	8.44	12.32	11.24
\checkmark \checkmark \checkmark \checkmark	78.51	89.68	80.44	4.00	5.52	5.76

Table 5: Ablations on other pre-trained weights.

Pre-trained Weights	Method	Dice (%) \uparrow		
		ET	WT	TC
CLIP	Full	64.58	84.69	73.31
	Ours	68.05	86.29	77.34
MAE	Full	64.86	84.71	73.95
	Ours	66.32	85.50	78.05
MoCo v3	Full	65.06	84.30	73.51
	Ours	67.09	85.45	77.41
SAM	Full	65.89	85.32	74.05
	Ours	67.64	86.10	78.33

Table 6: Ablations on MSD dataset with pre-trained Swin UNETR.

Organ	Method	Memory(GB) \downarrow	Time(h) \downarrow	Dice.AVG(%) \uparrow
Task02	Scratch	19.73	1.05	91.95
	Full	19.73	1.06	93.73
Heart (MRI)	Scratch	13.44	0.86	95.84
	Ours	13.44	0.86	95.84
Task06	Scratch	23.51	8.39	65.82
	Full	23.51	8.39	67.69
Lung (CT)	Scratch	20.30	8.03	78.09
	Ours	20.30	8.03	78.09
Task09	Scratch	20.32	3.21	95.76
	Full	20.32	3.21	96.52
Spleen (CT)	Scratch	19.71	2.22	97.06
	Ours	19.71	2.22	97.06

5. Conclusion

In this work, we present a new PET framework named Med-Tuning with strong generalization capabilities for the practical application of MVS. Taking advantage of both spatial relationship modeling (coarse/fine-grained) and volumetric correlations, our framework achieves better volumetric segmentation accuracy on 2D baselines pre-trained on relatively easily acquired natural images. To some extent, Med-Tuning could consistently and sus-

tainably boost the segmentation performance of pre-trained models on MVS tasks, keeping pace with the rapid development of foundation models in computer vision field.

Acknowledgments

Jianbo Jiao is supported by the Royal Society grants IES\R3\223050 and SIF\R1\231009.

References

- Michela Antonelli, Annika Reinke, Spyridon Bakas, Keyvan Farahani, Annette Kopp-Schneider, Bennett A Landman, Geert Litjens, Bjoern Menze, Olaf Ronneberger, Ronald M Summers, et al. The medical segmentation decathlon. *Nature communications*, 13(1):4128, 2022.
- Spyridon Bakas, Hamed Akbari, Aristeidis Sotiras, Michel Bilello, Martin Rozycki, Justin S Kirby, John B Freymann, Keyvan Farahani, and Christos Davatzikos. Advancing the cancer genome atlas glioma mri collections with expert segmentation labels and radiomic features. *Scientific data*, 4:170117, 2017.
- Spyridon Bakas, Mauricio Reyes, Andras Jakab, Stefan Bauer, Markus Rempfler, Alessandro Crimi, Russell Takeshi Shinohara, Christoph Berger, Sung Min Ha, Martin Rozycki, et al. Identifying the best machine learning algorithms for brain tumor segmentation, progression assessment, and overall survival prediction in the brats challenge. *arXiv preprint arXiv:1811.02629*, 2018.
- Hu Cao, Yueyue Wang, Joy Chen, Dongsheng Jiang, Xiaopeng Zhang, Qi Tian, and Manning Wang. Swin-unet: Unet-like pure transformer for medical image segmentation. In *European conference on computer vision*, pages 205–218. Springer, 2022.
- Shurong Chai, Rahul Kumar Jain, Shiyu Teng, Jiaqing Liu, Yinhao Li, Tomoko Tateyama, and Yen-wei Chen. Ladder fine-tuning approach for sam integrating complementary network. *arXiv preprint arXiv:2306.12737*, 2023.
- Shoufa Chen, Chongjian Ge, Zhan Tong, Jiangliu Wang, Yibing Song, Jue Wang, and Ping Luo. Adaptformer: Adapting vision transformers for scalable visual recognition. *Advances in Neural Information Processing Systems*, 35:16664–16678, 2022.
- Xinlei Chen, Saining Xie, and Kaiming He. An empirical study of training self-supervised vision transformers. *2021 IEEE/CVF International Conference on Computer Vision (ICCV)*, pages 9620–9629, 2021.
- Lu Chi, Borui Jiang, and Yadong Mu. Fast fourier convolution. *Advances in Neural Information Processing Systems*, 33:4479–4488, 2020.
- Özgün Çiçek, Ahmed Abdulkadir, Soeren S Lienkamp, Thomas Brox, and Olaf Ronneberger. 3d u-net: learning dense volumetric segmentation from sparse annotation. In *International conference on medical image computing and computer-assisted intervention*, pages 424–432. Springer, 2016.
- Jia Deng, Wei Dong, Richard Socher, Li-Jia Li, Kai Li, and Li Fei-Fei. Imagenet: A large-scale hierarchical image database. In *2009 IEEE conference on computer vision and pattern recognition*, pages 248–255. Ieee, 2009.

- Caiwen Ding, Siyu Liao, Yanzhi Wang, Zhe Li, Ning Liu, Youwei Zhuo, Chao Wang, Xuehai Qian, Yu Bai, Geng Yuan, et al. Circnn: accelerating and compressing deep neural networks using block-circulant weight matrices. In *Proceedings of the 50th Annual IEEE/ACM International Symposium on Microarchitecture*, pages 395–408, 2017.
- Alexey Dosovitskiy, Lucas Beyer, Alexander Kolesnikov, Dirk Weissenborn, Xiaohua Zhai, Thomas Unterthiner, Mostafa Dehghani, Matthias Minderer, Georg Heigold, Sylvain Gelly, et al. An image is worth 16x16 words: Transformers for image recognition at scale. In *International Conference on Learning Representations*, 2021.
- Marc Fischer, Alexander Bartler, and Bin Yang. Prompt tuning for parameter-efficient medical image segmentation. *Medical Image Analysis*, 91:103024, 2024.
- Ali Hatamizadeh, V. Nath, Yucheng Tang, Dong Yang, Holger R. Roth, and Daguang Xu. Swin unetr: Swin transformers for semantic segmentation of brain tumors in mri images. In *BrainLes@MICCAI*, 2022a.
- Ali Hatamizadeh, Yucheng Tang, Vishwesh Nath, Dong Yang, Andriy Myronenko, Bennett Landman, Holger R Roth, and Daguang Xu. Unetr: Transformers for 3d medical image segmentation. In *Proceedings of the IEEE/CVF Winter Conference on Applications of Computer Vision*, pages 574–584, 2022b.
- Kaiming He, Xinlei Chen, Saining Xie, Yanghao Li, Piotr Dollár, and Ross Girshick. Masked autoencoders are scalable vision learners. In *Proceedings of the IEEE/CVF Conference on Computer Vision and Pattern Recognition*, pages 16000–16009, 2022.
- Nicholas Heller, Niranjana Sathianathan, Arveen Kalapara, Edward Walczak, Keenan Moore, Heather Kaluzniak, Joel Rosenberg, Paul Blake, Zachary Rengel, Makinna Oestreich, et al. The kits19 challenge data: 300 kidney tumor cases with clinical context, ct semantic segmentations, and surgical outcomes. *arXiv preprint arXiv:1904.00445*, 2019.
- Neil Houlsby, Andrei Giurgiu, Stanislaw Jastrzebski, Bruna Morrone, Quentin de Larousilhe, Andrea Gesmundo, Mona Attariyan, and Sylvain Gelly. Parameter-efficient transfer learning for nlp. In *ICML*, 2019.
- Fabian Isensee, Paul F Jaeger, Simon AA Kohl, Jens Petersen, and Klaus H Maier-Hein. nnu-net: a self-configuring method for deep learning-based biomedical image segmentation. *Nature methods*, 18(2):203–211, 2021.
- Menglin Jia, Luming Tang, Bor-Chun Chen, Claire Cardie, Serge Belongie, Bharath Hariharan, and Ser-Nam Lim. Visual prompt tuning. In *European Conference on Computer Vision*, pages 709–727. Springer, 2022.
- Alexander Kirillov, Eric Mintun, Nikhila Ravi, Hanzi Mao, Chloe Rolland, Laura Gustafson, Tete Xiao, Spencer Whitehead, Alexander C Berg, Wan-Yen Lo, et al. Segment anything. In *Proceedings of the IEEE/CVF International Conference on Computer Vision*, pages 4015–4026, 2023.

- Jae-Han Lee, Minhyeok Heo, Kyung-Rae Kim, and Chang-Su Kim. Single-image depth estimation based on fourier domain analysis. In *Proceedings of the IEEE Conference on Computer Vision and Pattern Recognition*, pages 330–339, 2018.
- Shaohua Li, Kaiping Xue, Bin Zhu, Chenkai Ding, Xindi Gao, David Wei, and Tao Wan. Falcon: A fourier transform based approach for fast and secure convolutional neural network predictions. In *Proceedings of the IEEE/CVF Conference on Computer Vision and Pattern Recognition*, pages 8705–8714, 2020.
- Hao Liu, Xinghua Jiang, Xin Li, Antai Guo, Yiqing Hu, Deqiang Jiang, and Bo Ren. The devil is in the frequency: Geminated gestalt autoencoder for self-supervised visual pre-training. In *Proceedings of the AAAI Conference on Artificial Intelligence*, volume 37, pages 1649–1656, 2023a.
- Jie Liu, Yixiao Zhang, Jie-Neng Chen, Junfei Xiao, Yongyi Lu, Bennett A Landman, Yixuan Yuan, Alan Yuille, Yucheng Tang, and Zongwei Zhou. Clip-driven universal model for organ segmentation and tumor detection. In *Proceedings of the IEEE/CVF International Conference on Computer Vision*, pages 21152–21164, 2023b.
- Ze Liu, Yutong Lin, Yue Cao, Han Hu, Yixuan Wei, Zheng Zhang, Stephen Lin, and Baining Guo. Swin transformer: Hierarchical vision transformer using shifted windows. In *Proceedings of the IEEE/CVF international conference on computer vision*, pages 10012–10022, 2021.
- Bjoern H Menze, Andras Jakab, Stefan Bauer, Jayashree Kalpathy-Cramer, Keyvan Farahani, Justin Kirby, Yuliya Burren, Nicole Porz, Johannes Slotboom, Roland Wiest, et al. The multimodal brain tumor image segmentation benchmark (brats). *IEEE transactions on medical imaging*, 34(10):1993–2024, 2014.
- Fausto Milletari, Nassir Navab, and Seyed-Ahmad Ahmadi. V-net: Fully convolutional neural networks for volumetric medical image segmentation. In *2016 fourth international conference on 3D vision (3DV)*, pages 565–571. IEEE, 2016.
- Xing Nie, Bolin Ni, Jianlong Chang, Gaofeng Meng, Chunlei Huo, Shiming Xiang, and Qi Tian. Pro-tuning: Unified prompt tuning for vision tasks. *IEEE Transactions on Circuits and Systems for Video Technology*, 2023.
- A Oppenheim, Jae Lim, Gary Kopec, and SC Pohlig. Phase in speech and pictures. In *ICASSP'79. IEEE International Conference on Acoustics, Speech, and Signal Processing*, volume 4, pages 632–637. IEEE, 1979.
- Junting Pan, Ziyi Lin, Xiatian Zhu, Jing Shao, and Hongsheng Li. St-adapter: Parameter-efficient image-to-video transfer learning. *Advances in Neural Information Processing Systems*, 35:26462–26477, 2022.
- Adam Paszke, Sam Gross, Francisco Massa, Adam Lerer, James Bradbury, Gregory Chanan, Trevor Killeen, Zeming Lin, Natalia Gimelshein, Luca Antiga, et al. Pytorch: An imperative style, high-performance deep learning library. *Advances in neural information processing systems*, 32, 2019.

- Himashi Peiris, Munawar Hayat, Zhaolin Chen, Gary Egan, and Mehrtash Harandi. A robust volumetric transformer for accurate 3d tumor segmentation. In *International Conference on Medical Image Computing and Computer-Assisted Intervention*, pages 162–172. Springer, 2022.
- Alec Radford, Jong Wook Kim, Chris Hallacy, Aditya Ramesh, Gabriel Goh, Sandhini Agarwal, Girish Sastry, Amanda Askell, Pamela Mishkin, Jack Clark, Gretchen Krueger, and Ilya Sutskever. Learning transferable visual models from natural language supervision. In *International Conference on Machine Learning*, 2021.
- Yongming Rao, Wenliang Zhao, Zheng Zhu, Jiwen Lu, and Jie Zhou. Global filter networks for image classification. *Advances in Neural Information Processing Systems*, 34, 2021.
- Olaf Ronneberger, Philipp Fischer, and Thomas Brox. U-net: Convolutional networks for biomedical image segmentation. In *International Conference on Medical image computing and computer-assisted intervention*, pages 234–241. Springer, 2015.
- Julio Silva-Rodríguez, Jose Dolz, and Ismail Ben Ayed. Towards foundation models and few-shot parameter-efficient fine-tuning for volumetric organ segmentation. In *International Conference on Medical Image Computing and Computer-Assisted Intervention*, pages 213–224. Springer, 2023.
- Yi-Lin Sung, Jaemin Cho, and Mohit Bansal. Lst: Ladder side-tuning for parameter and memory efficient transfer learning. *Advances in Neural Information Processing Systems*, 35:12991–13005, 2022.
- Yucheng Tang, Dong Yang, Wenqi Li, Holger R Roth, Bennett Landman, Daguang Xu, Vishwesh Nath, and Ali Hatamizadeh. Self-supervised pre-training of swin transformers for 3d medical image analysis. In *Proceedings of the IEEE/CVF Conference on Computer Vision and Pattern Recognition*, pages 20730–20740, 2022.
- Constantin Ulrich, Fabian Isensee, Tassilo Wald, Maximilian Zenk, Michael Baumgartner, and Klaus H Maier-Hein. Multitalent: A multi-dataset approach to medical image segmentation. In *International Conference on Medical Image Computing and Computer-Assisted Intervention*, pages 648–658. Springer, 2023.
- Wenxuan Wang, Chen Chen, Meng Ding, Hong Yu, Sen Zha, and Jiangyun Li. Transbts: Multimodal brain tumor segmentation using transformer. In *International Conference on Medical Image Computing and Computer-Assisted Intervention*, pages 109–119. Springer, 2021.
- Junde Wu, Rao Fu, Huihui Fang, Yuanpei Liu, Zhaowei Wang, Yanwu Xu, Yueming Jin, and Tal Arbel. Medical sam adapter: Adapting segment anything model for medical image segmentation. *arXiv preprint arXiv:2304.12620*, 2023.
- Tete Xiao, Yingcheng Liu, Bolei Zhou, Yuning Jiang, and Jian Sun. Unified perceptual parsing for scene understanding. In *Proceedings of the European conference on computer vision (ECCV)*, pages 418–434, 2018.

- Mengde Xu, Zheng Zhang, Fangyun Wei, Han Hu, and Xiang Bai. Side adapter network for open-vocabulary semantic segmentation. In *Proceedings of the IEEE/CVF Conference on Computer Vision and Pattern Recognition*, pages 2945–2954, 2023.
- Taojiannan Yang, Yi Zhu, Yusheng Xie, Aston Zhang, Chen Chen, and Mu Li. Aim: Adapting image models for efficient video understanding. In *International Conference on Learning Representations*, 2023. URL https://openreview.net/forum?id=CIoSZ_HKHS7.
- Yanchao Yang and Stefano Soatto. Fda: Fourier domain adaptation for semantic segmentation. In *Proceedings of the IEEE/CVF conference on computer vision and pattern recognition*, pages 4085–4095, 2020.
- Rongtian Ye, Fangyu Liu, and Liqiang Zhang. 3d depthwise convolution: Reducing model parameters in 3d vision tasks. In *Advances in Artificial Intelligence: 32nd Canadian Conference on Artificial Intelligence, Canadian AI 2019, Kingston, ON, Canada, May 28–31, 2019, Proceedings 32*, pages 186–199. Springer, 2019.
- Jason Yosinski, Jeff Clune, Yoshua Bengio, and Hod Lipson. How transferable are features in deep neural networks? *Advances in neural information processing systems*, 27, 2014.
- Bruce XB Yu, Jianlong Chang, Lingbo Liu, Qi Tian, and Chang Wen Chen. Towards a unified view on visual parameter-efficient transfer learning. *arXiv preprint arXiv:2210.00788*, 2022.
- Ji Zhang, Shihan Wu, Lianli Gao, Hengtao Shen, and Jingkuan Song. Dept: Decoupled prompt tuning. *arXiv preprint arXiv:2309.07439*, 2023.
- Hong-Yu Zhou, Jiansen Guo, Yinghao Zhang, Xiaoguang Han, Lequan Yu, Liansheng Wang, and Yizhou Yu. nnformer: volumetric medical image segmentation via a 3d transformer. *IEEE Transactions on Image Processing*, 2023.
- Zongwei Zhou, Md Mahfuzur Rahman Siddiquee, Nima Tajbakhsh, and Jianming Liang. Unet++: A nested u-net architecture for medical image segmentation. In *Deep learning in medical image analysis and multimodal learning for clinical decision support*, pages 3–11. Springer, 2018.

Appendix A. Implementation Details.

A.1. Details about Benchmark Datasets

Details about BraTS 2019, BraTS 2020 and KiTS 2019 datasets are shown in Table 7.

A.2. Details about Benchmark Validation Experiments.

We employ pre-trained weights from two exemplary Transformer-based backbones, Swin Transformer tiny (Liu et al., 2021) pre-trained on ImageNet-1k and Vision Transformer base version (ViT-B/16) (Dosovitskiy et al., 2021) pre-trained on ImageNet-21k (Deng et al.,

Table 7: Details about BraTS 2019, BraTS 2020 and KiTS 2019 datasets.

Dataset	Modality	Number of Training Cases	Number of Test Cases	Spatial Resolution
KiTS 2019	CT	210	90	512×512
BraTS 2019	MRI	335	125	$240 \times 240 \times 155$
BraTS 2020	MRI	369	125	$240 \times 240 \times 155$

2009). Swin-UNet (Cao et al., 2022) and ViT (Dosovitskiy et al., 2021) with UPerNet (Xiao et al., 2018) decoder (ViT+UPerNet) are chosen as two robust baselines to ensure equitable comparison. As shown in Table 8, the specific implementation details on BraTS 2019, BraTS 2020, and KiTS 2019 datasets for two baselines are comprehensively illustrated. On all three benchmark datasets, models are fine-tuned with a batch size of 16 and the Adam optimizer.

During training, the following data augmentation techniques are applied to BraTS 2019 and BraTS 2020 datasets: (1) random cropping from $240 \times 240 \times 155$ to $128 \times 128 \times 128$ voxels; (2) random mirror flipping across the axial, coronal and sagittal planes by a probability of 0.5; (3) random intensity shift between $[-0.1, 0.1]$ and scale between $[0.9, 1.1]$. $L2$ Norm is also applied for regularization with a weight decay rate of 10^{-5} . As for the KiTS 2019 dataset, the employed data augmentations follow as the prior work (Isensee et al., 2021).

Table 8: Implementation details on BraTS 2019, BraTS 2020 and KiTS 2019 datasets for two baselines (i.e., Swin-UNet, ViT+UPerNet).

Dataset	Baseline	Backbone	Pre-trained Weight	Learning rate	Training epochs	Warm-up epochs
BraTS 2019 & BraTS 2020	Swin-UNet	Swin-T	ImageNet-1k	0.002	250	60
	ViT+UPerNet	ViT-B/16	ImageNet-21k	0.002	250	25
KiTS 2019	Swin-UNet	Swin-T	ImageNet-1k	0.002	500	20
	ViT+UPerNet	ViT-B/16	ImageNet-21k	0.004	500	20

A.3. Details about Generalization Capability Experiments.

We conduct ablation experiments to investigate the generalization capability of our Med-Tuning on the 3D baseline and pre-trained weight on the medical dataset. The Medical Segmentation Decathlon (MSD) (Antonelli et al., 2022) dataset includes 10 segmentation tasks covering various organs and image modalities. These tasks are intentionally diverse, presenting challenges like limited training data, class imbalances, multi-modality data, and small objects. In the main text, we have validated our approach on two MRI and one CT benchmark dataset. For ablation experiments, we selected one MRI and two CT datasets (i.e., Task02 Heart (MRI), Task06 Lung (CT), and Task09 Spleen (CT)) from the MSD dataset. Dataset pre-processing followed the protocol outlined in Swin UNETR (Tang et al., 2022). In Table 6, Memory(GB) represents memory usage during the fine-tuning,

Time(h) denotes the fine-tuning time, and Dice AVG signifies the average of multi-class Dice scores for the corresponding segmentation task.

A.4. The position of the inserted parameters.

Regarding the insertion position for the parameters, for SwinUnet-Tiny and SwinUNETR, we have incorporated the Med-Adapter exclusively within each transformer layer of their encoder. This results in a total of 8 Med-Adapters, calculated from 4×2 (number of stages \times number of layers in each stage). Within each stage, the second Med-Adapter is designated for Inter-FI. In the case of ViT+UPerNet, a Med-Adapter is inserted following every layer, amounting to a total of 12 (number of layers in ViT-B/16) Med-Adapters. Specifically, the Med-Adapters placed after the 2nd, 5th, 8th, and 11th layers are used for Inter-FI, maintaining a division of the ViT encoder into 4 stages, similar to the Swin Transformer setup. The relative positioning between Med-Adapters and Transformer blocks can be referenced in Figure 2 of our manuscript. Through our experiments, we have determined that the insertion position illustrated in Figure 2 of the manuscript represent the optimal configuration, as currently established.

A.5. The scale of bottleneck features of Med-Adapter.

As indicated in Table 9 of our manuscript, the default Reduction Ratio is set to 6. Consequently, for all baselines, the scale of the bottleneck features of the adapter is represented by $L/6$, L is the base scale of features in each stage (i.e., the scale of input features of Med-Adapter). Specifically, the scale of bottleneck features of 8 Med-Adapter in SwinUnet-Tiny or SwinUNETR are [16, 16, 32, 32, 64, 64, 128, 128]. The scale of bottleneck features of 12 Med-Adapter in ViT+UPerNet are both 128.

Appendix B. Visualization Comparisons

B.1. Visualization Comparisons with other PET method

Comparison with full fine-tuning, head tuning and previous PET methods in terms of the trade-off between the number of tuned parameters and segmentation accuracy is shown in Figure 3. The experiments were conducted using ViT+UPerNet as the baseline on the BraTS 2019 dataset. The horizontal axis represents the parameters involved in model training during the fine-tuning stage, while the vertical axis denotes the mean Dice scores for ET, WT, and TC. Our method achieves much better segmentation performance than full fine-tuning and previous state-of-the-art PET methods with much less tuned parameters.

B.2. Visualization of BraTS 2019

Qualitative results of BraTS 2019 datasets are shown in Figure 4, with the comparison with full fine-tuning, ST-Adapter and VPT. As the labels for the validation set are not available, five-fold cross-validation is conducted on the training set for visualization. Our method recognizes brain tumors in enhancing and non-enhancing regions more accurately and reduces missed or false identification of the peritumoral edema in general.

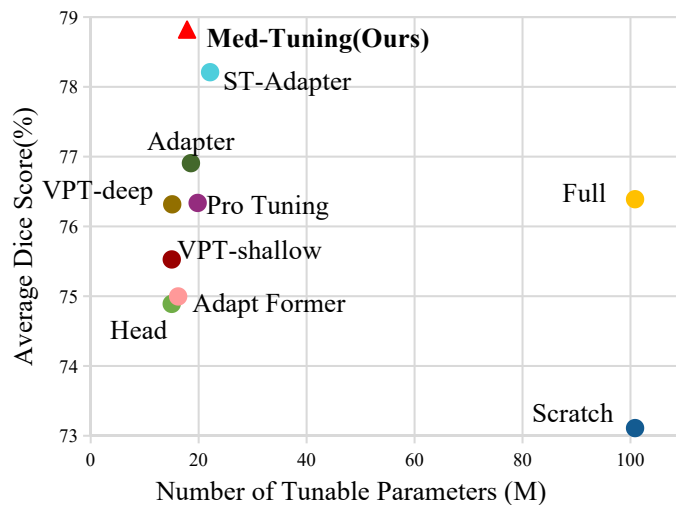


Figure 3: Comparison with previous PET methods in terms of the number of tuned parameters and Dice scores.

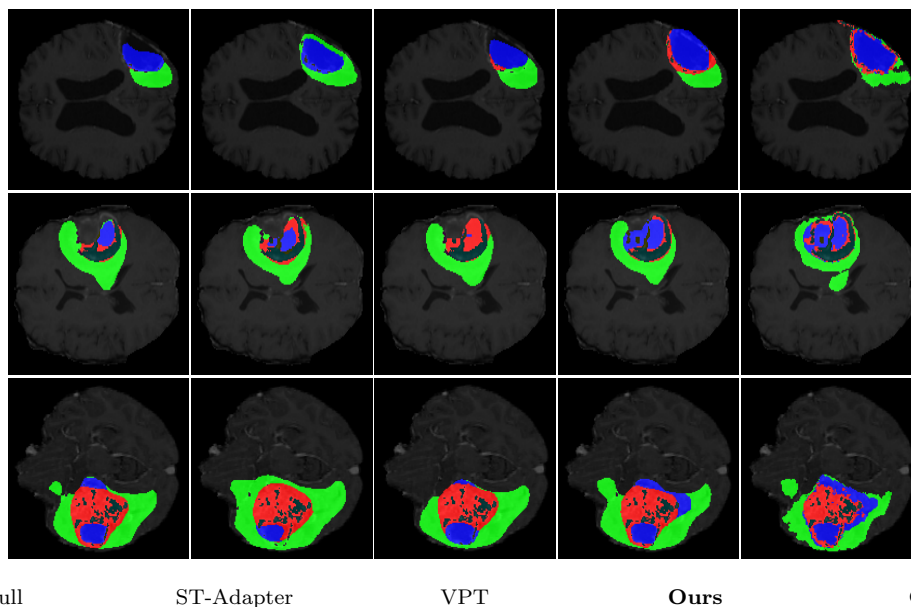


Figure 4: The visual comparison of segmentation results on BraTS 2019. The blue, red and green regions denote the enhancing tumors, non-enhancing tumors, and peritumoral edema. GT=Ground Truth.

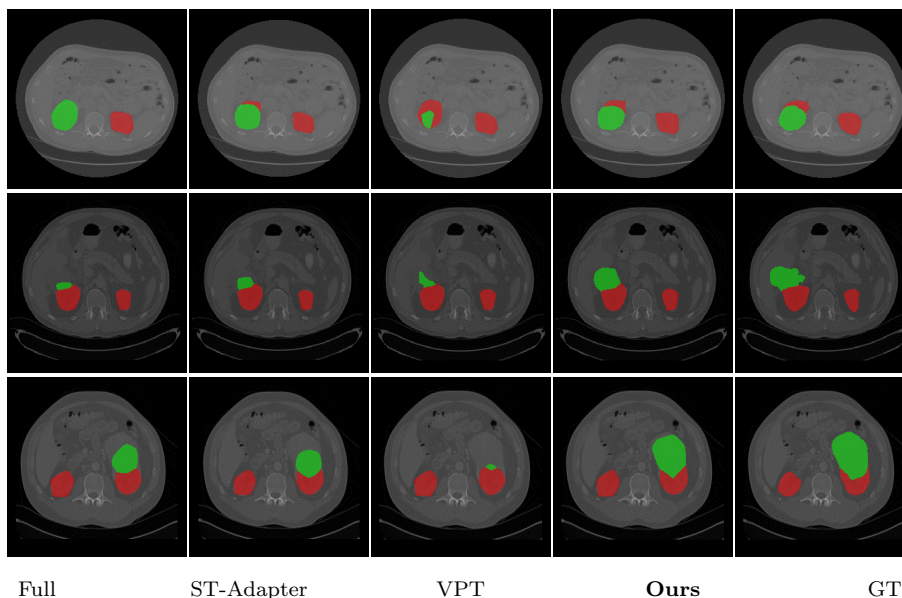


Figure 5: The visual comparison of segmentation results on KiTS 2019. The red and green regions denote the kidneys and kidney tumors. GT=Ground Truth.

B.3. Visualization of KiTS 2019

As the labels for the validation set are not available, five-fold cross-validation is conducted on the training set for visualization. The qualitative results of KiTS 2019 datasets, depicted in Figure 5, highlight the superior performance of our method in organ and tumor segmentation compared to full fine-tuning, ST-Adapter, and VPT. Our approach demonstrates enhanced accuracy in segmenting organs and tumor types, producing finer-grained segmentation masks for corresponding tumors.

Appendix C. More Ablation Studies and Analysis

C.1. Reduction Ratio in Bottleneck Design.

Method	Tuned Params(M)	Inserted Params(M)	Dice (%) \uparrow			
			ET	WT	TC	Avg.
$\alpha=2$	10.064	3.313	76.89	90.14	81.92	82.99
$\alpha=4$	7.994	1.243	77.22	90.09	81.59	82.97
$\alpha=6$	7.489	0.738	77.06	90.28	82.71	83.35
$\alpha=8$	7.271	0.520	76.94	89.62	80.74	82.44

Table 9: Ablation study on reduction ratio α . Swin-UNet with Swin-T pre-trained on supervised ImageNet-1k.

We analyze the effect of different reduction ratios of the bottleneck structure in our Med-Adapter. Note that the reduction ratio α here is a key factor that influences the tuned parameters introduced by our Med-Adapter. Four diverse settings of α are selected. As shown in Table 9, Med-Tuning achieves a promising trade-off between segmentation accuracy and the tuned parameter costs with $\alpha = 6$. On this basis, higher α would cause inferior model performance because of the deteriorated representation capability with limited tuned parameters, while lower α would lead to a certain degree of information redundancy and a sharp increase of tuned parameters, resulting in both decreased segmentation accuracy and high training costs.

C.2. Design for Global Dependency Modeling.

Table 10: Ablation study on different designs for global dependency modeling. The baseline is Swin-UNet with Swin-T pre-trained on supervised ImageNet-1k. DWConvK denotes depth-wise convolution with a kernel size of $K \times K$.

Method	Tuned Params(M)	Inserted Params(M)	Dice (%) \uparrow			
			ET	WT	TC	Avg.
DWConv9	7.837	1.086	76.48	90.58	81.10	82.72
DWConv11	8.126	1.375	76.82	89.40	80.05	82.09
FFT	7.994	1.243	77.22	90.09	81.59	82.97

In order to pursue the most effective and parameter-efficient architecture of our proposed Med-Adapter, we also investigate different designs for the global branch in our Med-Adapter block to achieve global dependency modeling. Since convolutional blocks with a large kernel size or self-attention are usually adopted by previous works for global contextual modeling and the baseline Swin-UNet itself consists of plenty of self-attention operation in each local window, we take the depth-wise convolution with a kernel size of 9 and 11 separately to replace our originally employed Fast Fourier Transform (i.e., FFT) branch for a comprehensive comparison. The comparison of the segmentation performance and tuned model parameters is shown in Table 10. It can be noticed that by taking advantage of the parameter-efficient FFT branch for effective long-range context modeling, the architecture with the FFT branch achieves the optimal trade-off between model performance and tuned parameters, reaching the best segmentation accuracy with only 1.243M introduced model parameters. In contrast, too large kernel size of the employed convolutions (i.e., DWConv11) will result in a burdensome model structure and a large amount of tuned parameter cost.

C.3. Intra-FE Module Design.

We first probe into the rationale of the proposed Intra-FE Module without Inter-FI on Swin-UNet baseline. Swin-UNet with Swin-T pre-trained on supervised ImageNet-1k is taken as a baseline. As presented in Table 11, the introduction of MLB, FGB, or channel mixing consistently leads to a considerable performance increase. Specifically, with only 0.002M additional tuned parameters, the FGB branch greatly improves the segmentation

Table 11: Ablation study on Intra-FE. The first row is the result of the Vanilla Adapter.

MLB	FGB	$Conv_{1\times 1\times 1}$	Tuned Params(M)	Inserted Params(M)	Dice (%) \uparrow		
					ET	WT	TC
-	-	-	7.541	0.790	75.13	87.50	75.29
\checkmark	-	-	7.574	0.823	75.19	89.44	80.89
\checkmark	\checkmark	-	7.577	0.825	75.30	89.93	81.93
\checkmark	\checkmark	\checkmark	7.675	0.924	77.10	90.05	81.02

Table 12: Ablation study on inter-FI.

Method	Tuned Params(M)	Inserted Params(M)	Dice (%) \uparrow		
			ET	WT	TC
Add	7.896	1.144	75.79	88.99	79.00
Max	7.896	1.144	75.22	89.72	81.41
Concat	7.994	1.243	77.22	90.09	81.59

accuracy, showing the effectiveness and parameter efficiency of our employed FGB branch. Additionally, channel mixing further boosts the performance by a large margin, especially on ET (\uparrow 1.80%).

C.4. Inter-FI Module Design.

After investigating the effect of the intra-stage feature enhancement, we further verify the effectiveness of the inter-stage feature interaction, as shown in Table 12. Compared with the intra-only structure (i.e., without the feature connectivity between adjacent Med-Adapters), the model with inter-stage achieves a considerable performance gain with only 0.319M extra parameters for feature alignment among adjacent stages, showing the effectiveness of our inter-stage interaction. Unlike concatenation which maintains the feature representations of different stages as much as possible, direct addition or taking the maximum value (at each pixel) of neighboring feature maps with diverse semantic levels would unintentionally degrade the original feature representation, resulting in a sharp decrease in segmentation performance.

C.5. Decoder Design.

Here we explore the effect of different decoder designs in our architecture. Although the backbone is frozen and only the inserted Med-Adapters as well as the decoder are updated during fine-tuning, the essentially tuned model parameters introduced by the segmentation decoder can not be reckoned as negligible. In other words, to pursue an extremely PET framework, the design of the employed decoder should be sufficiently lightweight with strictly controlled model parameters. Thus, various segmentation decoders with greatly varied model complexity are introduced respectively for a thorough analysis. As shown in Table 13, ViT-B/16 with the SETR-MLA decoder reaches the best trade-off between segmentation accuracy and tuned parameter costs, benefiting from the effective multi-scale

Table 13: Ablation study on decoder design. ViT-B/16 is pre-trained on supervised ImageNet-1k.

Method	Tuned Params(M)	Decoder Params(M)	Dice (%) \uparrow			
			ET	WT	TC	Avg.
UPerNet (Default)	19.562	15.095	68.27	87.22	81.63	79.04
U-Net	9.269	4.712	67.68	88.08	81.72	79.16
SETR-MLA	8.347	3.790	68.12	87.91	81.98	79.34
SETR-Naive	5.004	0.447	69.11	86.93	81.71	79.25
SETR-PUP	5.200	0.643	68.55	86.51	80.42	78.49

feature aggregation. Besides, taking the simplest SETR-Naive that is composed of a convolution and an interpolation operation for upsampling as the decoder leads to the lowest tuned parameters 5.004M while achieving promising segmentation performance with an average Dice score of 79.34%. It can be seen from Table 13 that although the decoder size dominantly decides the overall tuned parameters, it does not show a direct impact on model performance.

C.6. Data Efficiency.

Table 14: Ablation study on data efficiency property with pre-trained ViT-B/16.

Dataset Ratio	Method	Memory Cost (GB) \downarrow	Training Time (h) \downarrow	Dice (%) \uparrow			HF (mm) \downarrow		
				ET	WT	TC	ET	WT	TC
100%	Full	16.55	1.34	68.04	85.74	76.58	6.94	7.28	7.99
100%	Ours	13.53	1.20	75.46	86.80	86.24	3.78	6.94	4.34
75%	Ours	13.53	1.05	69.12	86.69	78.06	6.33	6.01	6.63
50%	Ours	13.53	0.72	69.19	86.26	77.26	6.28	7.03	7.12
25%	Ours	13.53	0.39	67.43	85.64	74.57	6.32	7.71	8.14
5%	Ours	13.53	0.17	59.61	80.44	64.01	15.07	16.64	16.36

At last, we also explore the data efficiency property of our method by examining performance across various training data ratios, particularly in low-data settings. Table 14 shows the quantitative comparison with different numbers of training samples. Our Med-Tuning can already achieve comparable performance to full fine-tuning using only **25%** training data. As the scale of training data increases, our method consistently improves the segmentation accuracy, with reduced training time and memory cost compared with full fine-tuning.

C.7. Other Weight Pre-trained on Medical Image Datasets.

Med-Tuning is not solely focused on pushing SOTA. Instead, it allows us to capitalize on the extensive progress made in natural image processing. This perspective underscores our

belief in the potential and value of integrating advancements from one domain to enhance the capabilities and applications in another.

Indeed, as highlighted in recent literature (Liu et al., 2023b; Silva-Rodríguez et al., 2023; Ulrich et al., 2023), there have been significant advancements in the field of medical image pre-trained models. Nevertheless, due to the considerable constraints of time, monetary resources, and clinical applicability faced by many researchers working on medical image pre-training, the pace of updates and the scale of medical image pre-training efforts still trail behind those in the natural image domain. Additionally, the use of many open-source codes in the medical imaging field presents a high threshold. Therefore, the vast array of convenient and accessible large-scale pre-trained weights from the natural image domain have become our primary choice.

Based on the above choices, we hypothesize that: If Med-Tuning can tackle the more challenging task of a large domain shift from features pre-trained on natural 2D images to CT/MRI volumes, then it is also capable of addressing the comparatively easier task of domain shift from features pre-trained on medical images to CT/MRI volumes. The experimental results in our manuscript have demonstrated the feasibility of a broader transfer process, thereby validating the effectiveness of our proposed approach in achieving the former scenario.

Regarding the latter scenario, we conducted experiments using the same baselines and pre-trained weights as those in (Liu et al., 2023b; Silva-Rodríguez et al., 2023), following our default training setting. The comprehensive results of all experiments are depicted in Table 15.

Table 15: The comparison between original SwinUNETR, Universal Model and our proposed Med-Tuning. The performance is evaluated by average Dice scores. "W1" signifies the use of the model and pre-training weights from (Tang et al., 2022), while "W2" references the model and pre-training weights from (Liu et al., 2023b). "SCR" denotes the model is trained from scratch and "FULL" denotes the full fine-tuning method. The first two columns of scores were directly copied from (Liu et al., 2023b). The last four columns of scores were obtained through training using our framework.

Dataset	SwinUNETR (SCR)	Universal Model (FULL)	Ours (SCR)	Ours (FULL, W1)	Ours (Med-Tuning, W1)	Ours (FULL, W2)	Ours (Med-Tuning, W2)
Task06 Heart	68.90	67.15	65.82	67.69	78.09	68.37	78.53
Task09 Heart	95.80	96.71	95.76	96.52	97.06	96.35	97.60

From our results, Med-Tuning proves to be capable of consistently improving the precision in medical volumetric segmentation tasks by using medical pre-trained weights, requiring only a small number of training parameters for this enhancement. Besides, the trends observed in our experimental results suggest that our proposed approach can keep pace

Table 16: Comparisons of training time (hours) on BraTS2019 with SwinUnet and ViT+UPerNet backbone.

Method	ViT+UPerNet	SwinUnet
Scratch	1.74h	1.26h
Full	1.73h	1.26h
Head	1.28h	1.02h
VPT-Shallow	1.09h	0.98h
VPT-Deep	1.18h	1.01h
Adapter	1.77h	1.30h
AdaptFormer	1.44h	1.18h
Pro-tuning	1.84h	1.47h
ST-Adapter	1.79h	1.55h
Ours	1.88h	1.51h

with the development of visual models pre-trained in medical domain, aligning with the conclusions drawn at the end of our manuscript.

Finally, we would like to add that as demonstrated in our results shown in Table 10, using the W2 weights improved the Dice score by 0.6 over the W1 weights. Hence, we also look forward to the widespread development of large-scale pre-trained models like (Liu et al., 2023b) in medical domain and are excited about the potential to further enhance their performance using our Med-Tuning.

C.8. Training Time.

Under default training settings, the training time of each method are listed in Table 16. The results indicate that the introduction of few new training parameters inevitably results in a slight increase in training. However, we achieves a commendable balance between training time cost and the tuning of parameters.